JOURNAL OF Applied Polymer SCIENCE

Electrical and Mechanical Properties of the Potassium Permanganate Treated Short Sisal Fiber Reinforced Epoxy Composite in Correlation to the Macromolecular Structure of the Reinforced Fiber

Annapurna Patra,[1] Dillip K. Bisoyi,[1] Prem K. Manda,[2] A. K. Singh[2]
[1]Department of Physics, NIT Rourkela, Rourkela, Orissa 769008, India
[2]Material Science Division, DMRL Hyderabad, Hyderabad, Andhra Pradesh 500058, India
Correspondence to: A. Patra (E-mail: annapurna.patra@gmail.com)

ABSTRACT: Sisal fibers are treated with potassium permanganent ($KMnO_4$)—acetone solution for various concentrations for different soaking time period prior to the composite fabrication. Small angle X-ray scattering (SAXS) and wide angle X-ray diffraction (WAXD) analysis shows significant change in the macromolecular and the crystallographic parameters of the fiber, respectively, after the treatment. Fiber treated with 0.05% $KMnO_4$-acetone solution for 2 min (05K2) is found to have highest degree of crystalinity, crystallite size, and bulk density. Enhanced tensile and flexural strength of the 05K2 reinforced epoxy composite (05KC2) is attributed to the increase surface roughness of the fiber. Lower values of dielectric constant (ε_r), dielectric loss (tan δ) and improved volume resistivity (ρ) for the 05KC2 composite may be due to the hindered molecular motion of the polymeric chains at the composite interface resulting from the better interlocking between the fiber and matrix. © 2012 Wiley Periodicals, Inc. J. Appl. Polym. Sci. 000: 000–000, 2012

KEYWORDS: SAXS; adhesion; defects; electrical properties; mechanical properties

Received 13 February 2012; accepted 13 June 2012; published online
DOI: 10.1002/app.38195

INTRODUCTION

Recent environmental concern and health hazards associated with the conventional synthetic fibers like glass, carbon, aramid, etc. have forced the manufacturing industries and scientists of fundamental research to develop an alternative reinforcing material. In this regard, the abundantly available natural plant fiber with low density, low cost, biodegradability, nontoxicity has been proved to be a boon in the present energy crisis situation.[1] Natural fiber reinforced composite not only gaining attention in substituting the synthetic fiber in conventional structural, automotive applications but also found to be suitable in many electrical applications like in suspension insulators, switch boards, antistatic applications, etc.[2] Among all the natural fibers, sisal fiber which is widely used as yarns ropes, twines, carpets is found to be most suitable for the applications in polymer composites because of its superior properties like high cellulose content, high tensile strength, and yet cheaper in price.[3]

However, the inherent hydrophilic nature of the sisal fiber leads to the poor compatibility with hydrophobic matrix hence creates hindrance for its full exploitation in the composite manufacturing industries.[4] Chemical and physical modifications of the fiber are found to be an effective method to improve the compatibility between the matrix and the reinforcing fiber, either by modifying the surface of the fiber or generating some new functional groups which can form bond with the matrix.[5]

SAXS is a powerful technique to characterize the structural changes and strain produced in a polymer along with the changes in the macromolecular parameters.[6,7] This analysis helps in understanding the structure–property relationship of the polymer and tailor-making the technology for mass production of different polymeric materials, especially fiber and fiber-reinforced composites by having a deeper understanding at the macromolecular level. Moreover, it can estimate the percentage of matter phase, void phase and many more macromolecular parameters of the fiber which can affect the strength, durability and stability of the fiber.[8]

Among the various chemical modifications, the $KMnO_4$ treatment on the fiber is known to be very effective in improving the bonding at the interface.[9] $KMnO_4$ is well known as a strong oxidizing agent. George et al. studied the effect of $KMnO_4$ treatment on the pineapple leaf fiber reinforced polyethylene composites and noticed the improvement in the mechanical properties

Additional Supporting Information may be found in the online version of this article.

after the treatment.[10] $KMnO_4$-treated banana fiber proved to be responsible for the higher thermal stability due to cellulose-manganet.[11] Khan et al. studied the effect of $KMnO_4$ treatment on the photo cure coir fiber which increases the tensile strength due to the strong oxidizing effect of $KMnO_4$ on the cellulose molecules in the fiber.[12] The dependence of the volume resistivity on the concentration of $KMnO_4$-treated sisal fiber reinforced low-density polyethylene was studied by Paul et al.[13] The strength and stiffness of the fiber provided by the cellulose gets modified during the chemical treatment.[14] Hence, it is essential to know the structural changes caused by chemical modifications. An understanding of the structural parameters of the fiber is also extremely important to assess the suitability of the fiber as well as the fiber reinforced composite in various potential applications.

The literature survey suggests that there is hardly any report on the study of macromolecular parameters of the $KMnO_4$-treated sisal fiber in correlation to the electrical and mechanical properties of the short sisal fiber reinforced epoxy composites. Dewaxing of the sisal fiber is effective in increasing the reinforcing efficiency of the fiber in epoxy.[15] Hence this article aims in further improvement in the reinforcing efficiency of the composite system by pretreating the sisal fiber with the combined effect of dewaxing and $KMnO_4$. This work investigates the effect of $KMnO_4$-treated dewaxed sisal fiber on the mechanical and electrical properties of the short sisal fiber reinforced epoxy composite along with a special emphasis on the macromolecular and crystallographic parameters of the reinforced fiber.

MATERIALS AND METHODS

Sisal fiber was obtained from the Sisal Research Station, Indian Council of Agricultural Research, Bamara, Orissa, India having a diameter of 170–300 μm. Unmodified liquid epoxy resin based on Bisphenol A, of grade LY 556 along with hardener HY 951 was provided by B. Mukesh & Co., Kolkata, India. The density of the resin used in this work was 1.15 g/cc, whereas the hardener density was 0.97 g/cc. The various chemicals such as $KMnO_4$, acetone, acetic acid, alcohol, benzene (Merk) were used for the treatment of fiber.

Treatment of Fiber

The as received sisal fibers were dewaxed in a mixture of (1:2) ethanol and benzene for removing the surface impurities, as done earlier by Roy,[16] for 12 h so that it attains a hohlraum character, the substances lying in layers with free spaces in between.[17] For the $KMnO_4$ treatment the dewaxed fibers (80 g) were soaked in 1liter $KMnO_4$-acetone solution having various concentrations of $KMnO_4$ (0.01, 0.05, and 0.1%) for the period of 1, 2, and 3 min. After that the solution was decanted and the fibers were washed with acetone to remove excess solution present in the fiber. Finally fibers were dried at 60°C in the oven for 12 h. The $KMnO_4$-treated fibers are designated as 01K1, 05K1, 1K1, 01K2, 05K2, 1K2, 01K3, 05K3, and 1K3. The K symbolizes $KMnO_4$ treatment. The prefixes of K denote the concentration of $KMnO_4$ acetone solution, i.e., 01, 05, 1 for 0.01, 0.05, and 0.1% concentrations, respectively. However, the suffixes of K denotes the soaking time for the fiber in the solution in minutes. The untreated fiber was denoted as UT.

Fabrication of Composite Plate

The method for fabrication of all the composite is described elsewhere.[15] The untreated and $KMnO_4^-$ treated sisal fiber reinforced epoxy composites (KSFREC) are designated as UTC and 01KC1, 05KC1, 1KC1, 01KC2, 05KC2, 1KC2, 01KC3, 05KC3, and 1KC3, respectively. Here KC symbolizes for the $KMnO_4$-treated sisal fiber reinforced composite.

CHARACTERIZATIONS

The room temperature, smeared out, SAXS data of the raw and treated sisal fibers were obtained from SAXS 896986 Anton Paar which was mounted on Panalytical X-ray generator (PW3830). The setup was operated at 40 kV and 50 mA with Cu target. The sample to detector distance "a" was maintained at 310 mm.

Normally, X-ray Scattering takes place due to the difference in the electron density inside the particle. The electron density map tells about the defects in the crystal system in the sample. Because of the little difference in the electron density ($\Delta\eta$) between crystalline phase and amorphous phase, these two are taken as one phase, i.e., matter phase whereas void is as another phase. The electron density difference between these two phases is high. The idea of taking sisal fiber as a two phase system is due to the difference in electron density of matter phase and void phase.[18] In this study we have treated the sisal fiber as a nonideal two phase system and are also justified. The relevant theory and methods of evaluation of macromolecular parameters are described elsewhere.[19] All the computational analyses for the calculation of correlation functions and various macromolecular parameters have been carried out through self-developed FORTRAN programming.

To identify the effect of treatment on the crystallographic parameters of the sisal fiber, wide angle X-ray diffraction (WAXD) spectra were collected by PHILIPS PANalytical PW1830 with Cu-K_α radiation in the angular range from 5 to 45° with a scan speed of 0.04° s^{-1}. Chemical compositions of the raw and $KMnO_4$-treated fibers are investigated by the Perklin–Elmer FTIR spectrometer spectrum RX-1in the mid IR range, i.e., from 400 to 4000 cm^{-1}. The density measurements of the fiber were done as per ASTM D3800-99 by employing Archimedes principle. The surface morphology of sisal fibers and the composites were examined by SEM (JEOL JSM- 6480 LV). In order to evaluate the flexural strength and tensile strength of the composites three point bending test and tensile test were carried out by INSTRON 1195, respectively. The randomly oriented UTC and KSFREC specimens were cut as per the ASTM D790 and ASTM D3039 to measure the flexural strength and tensile strength, respectively. The sample dimensions for the flexural measurements was (130 × 30 × 5) mm cube with a crosshead speed of 2 mm/min with a gauge length of 50 mm whereas for the tensile measurements the sample it was (200 × 30 × 5) mm cube with crosshead speed of 1 mm/min with gauge length of 120 mm. The reported data were the average of the five successful tests. For electrical measurements, disk shaped composite samples having 15 mm diameter were cut out of the composites and were polished to make a thickness of 2 mm. The

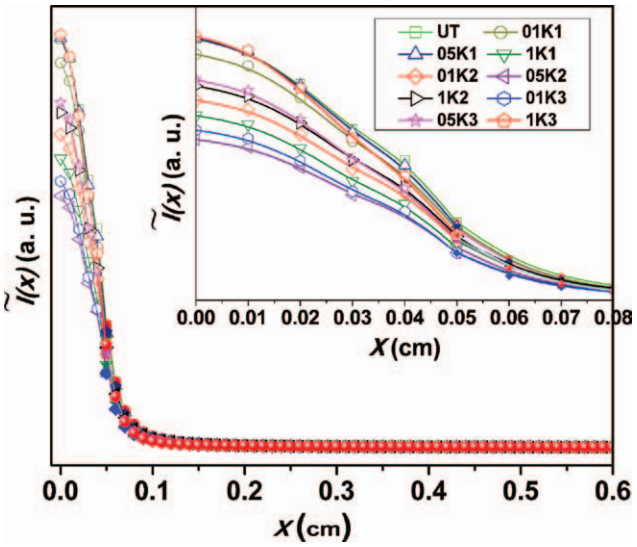

Figure 1. Background-corrected, smeared-out scattering curves for raw and $KMnO_4$-treated sisal fibers. Inset: Magnified view of the extrapolated scattering curve. [Color figure can be viewed in the online issue, which is available at wileyonlinelibrary.com.]

surfaces of the test samples were polished and coated with conductive silver paste.

The electrical measurements of the composites in this study were performed by using a computer interfaced LCR HITESTER with a frequency range of (1 Hz–1 MHz) at room temperatures. The dielectric constant (ε_r) was calculated from the capacitance using the following equation: $\varepsilon_r = Ct/\varepsilon_0 A$, where ε_r is the dielectric constant of the material, ε_0 is the permittivity of air, C is the capacitance, A is the area of cross section of the sample, and t is the thickness of the sample. The volume resistivity (ρ) the composites were calculated from the resistance using the equation: $\rho = RA/t$, where R is resistance, A is the area of cross section of the sample, and t is the thickness of the sample.

RESULTS AND DISCUSSION

Figure 1 exhibits the diffuse scattering curves of the untreated fiber and $KMnO_4$-treated fibers. The background corrected intensities are used for the analysis of the SAXS data. Five background corrected intensities near the origin are fitted to the following Gaussian curve by least square technique.

$$\tilde{I}(x \to 0) = p \cdot \exp(-qx^2) \tag{1}$$

Here, $\tilde{I}(x)$ is the smeared out intensity and x is the positions co-ordinate of the scattered intensity from the centre of the primary beam, where $x = 2a\theta$ and 2θ is the scattering angle. The values of constants p and q are used to extrapolate the scattering curve up to $x = 0$. The extrapolation is necessary as it is practically impossible to get the scattering curve up to $x = 0$. The extrapolated points are indicated by hollow symbols in the inset graph of Figure 1. These smeared out intensities and x shown in Figure 1, are required to find out the macromolecular parameters in subsequent analysis.

The method of extrapolation shown in Figure 1(inset) does not disturb the position and height of the 1st subsidiary maxima of the one dimensional correlation function $C_1(y)$.[21] The symmetry of the intensity pattern confirms the isotropic behavior of the sisal fiber.

Previous works on the lignocellulosic fiber suggest that the areas of cellulose production near the protoplasm are related to each other in some order. Hence form the cellulose molecules with some order to each other with high degree of orientation. This leads to the kind of isotropic lamellar structure.

The 3D correlation function $C(r)$ which contains the valuable information regarding macromolecular structural parameters is defined as the ratio of the average of the product of the electron density across the two ends of a virtual rod moving inside the particle to the average of the product when the length reduces to zero at the origin. It gives information about the nature of the phases present in the particle. The above function $C(r)$ is governed by the following relation.

$$C(r) = \frac{\int_0^\infty x\tilde{I}(x)J_0\left(2\pi rx/\lambda a\right)dx}{\int_0^\infty x\tilde{I}(x)dx} \tag{2}$$

Here J_0 is the Bessel function of Zero order first kind. The value of $C(r)$ normalizes to unit at the origin and decreases to zero when r attains the boundary of the particle, i.e., $r = R$, corresponding to the maximum displacement. This correlation function contains the information about the particle in three dimensions hence known as 3D correlation function.

The one-dimensional correlation function $C_1(y)$ can be visualized as a measuring rod of length "y" perpendicular to the layers which moves along the y-direction. In this study there is

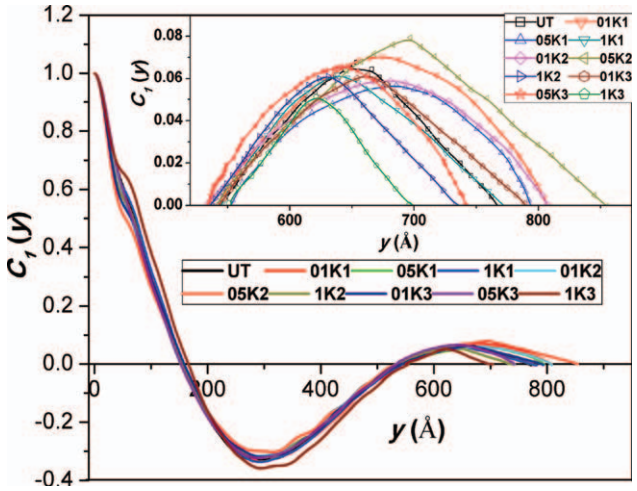

Figure 2. Variation of one dimensional correlation function C_1 (y) as a function of y for the raw and $KMnO_4$-treated fibers. Inset: Magnified view of first subsidiary maximum of one-dimensional correlation functions corresponding to the periodicity transverse to the layer. [Color figure can be viewed in the online issue, which is available at wileyonlinelibrary.com.]

significant contribution of $C_I(y)$ as sisal is having the lamellar structure. The expression for the one-dimensional correlation function $C_I(y)$ for layer structure in terms of x is expressed as

$$C_1(y) = \frac{\int_0^\infty x\tilde{I}(x)[J_0(z) - zJ_1(z)]dx}{\int_0^\infty x\tilde{I}(x)dx} \quad (3)$$

where $z = 2\pi xy/\lambda a$ and J_1 is the Bessel function of first order first kind.

The isotropic lamellar structure of all the investigated fiber samples justifies taking of one dimensional correlation, $C_I(y)$ function.[18] $C_I(y)$ of all the fibers for various values of y are computed and the plots are given in the Figure 2. According to Vonk[22] the position of first subsidiary maximum in the one-dimensional correlation function$C_1(y)$, gives the value of the average periodicity transverse to layers (D). Inside the fiber, the matter phase and void phase are thought to be arranged in terms of lamellar stack and each lamellar having some periodicity displays information about the specific inner surface area (S/V) of those lamellar stacks. It is also defined as phase boundary per unit volume of the dispersed phase.

$$S/V = 2/D \quad (4)$$

The values of D (average periodicity transverse to the layer correspond), specific inner surface area (S/V) calculated from each curve of the Figure 2 has been listed in Table I. The value of D is found to be highest for the 05K2 sample with least specific inner surface area.

The extent of matter and void phase inside the fiber are represented by $\bar{l}_1$and $\bar{l}_2$, respectively, whereas the volume fractions of matter and void phase are denoted by φ_1 and φ_2, respectively. Here, $\bar{l}_1$and $\bar{l}_2$ are calculated by using the relations $\bar{l}_1 = 4\varphi_1(V/S)$ and $\bar{l}_2 = 4\varphi_2(V/S)$which are presented in Table I. From Table I it is found that the values of $\bar{l}_1$and φ_1 are highest for 05K2 samples, but the values of φ_2 and $\bar{l}_2$are least for the same sample. The maximum value of $\bar{l}_1$and φ_1 for the sample 05K2 shows the increment in the matter phase. It may be due to the removal of the lignin, impurities and the waxy material from the interfibrillar regions of the fiber. The cellulose micro fibril gets rearranged properly decreasing the volume fraction of the void content "φ_2". The decrease in void content increases the mechanical properties of the fiber.[23] The transversal lengths of matter and void phases for a two-phase three-dimensional system were derived by Mittelbach and Porod and are given by the relation

$$1/\bar{l}_r = 1/\bar{l}_1 + 1/\bar{l}_2 \quad (7)$$

where $\bar{l}_r$is the range of inhomogeneity which has same meaning with that of reduced mass in mechanics.

The decrease in the value of $\bar{l}_r$with the increase in soaking period of the fiber in the $KMnO_4$ solution indicates the decrease in the disorderness inside the fiber due to the rearrangement of cellulose chains.[18] Out of all the samples, the fiber treated with

Table I. Various Macromolecular Parameters of Raw and $KMnO_4$-Treated Sisal Fibers Derived from SAXS Study

Macromolecular parameter	UT	01K1	05K1	1K1	01K2	05K2	1K2	01K3	05K3	1K3
R (10^{-4} Å^{-2})	8.831	10	9.931	8.052	9.002	11.109	7.354	8.573	9.093	6.813
D (Å)	654	674	686	637	680	696	630	664	642	621
S/V (10^{-3} Å^{-1})	3.0581	2.967	2.915	3.139	2.941	2.873	3.174	3.012	3.115	3.220
E_v(Å)	21.081	22.133	23.238	23.152	23.078	22.686	25.073	23.056	22.089	25.22
E_r (Å)	19.792	19.663	19.616	19.251	19.399	19.331	18.867	19.711	19.154	19.466
Φ_1	82.601	84.358	84.646	80.939	84.468	87.339	80.800	83.398	82.55	79.189
Φ_2	17.399	15.642	15.354	19.061	15.532	12.661	19.200	16.602	17.45	20.811
$\bar{l}_1$(Å)	1080.421	1137.145	1161.343	1031.162	1148.764	1215.758	1018.080	1107.525	1059.942	983.527
$\bar{l}_2$(Å)	227.578	210.854	210.656	242.837	211.235	176.241	241.9200	220.474	224.058	258.472
$\bar{l}_r$(Å)	187.982	177.872	178.312	196.549	178.426	153.927	195.471	183.871	184.959	204.681
l_c	351.097	314.736	313.879	325.976	311.374	299.084	318.62	323.666	327.916	322.513
$2E_v/D$ (%)	6.446	6.567	6.774	7.269	6.787	6.518	7.959	6.944	6.881	8.122
σ	0.013	0.014	0.012	0.014	0.013	0.016	0.007	0.008	0.023	0.007

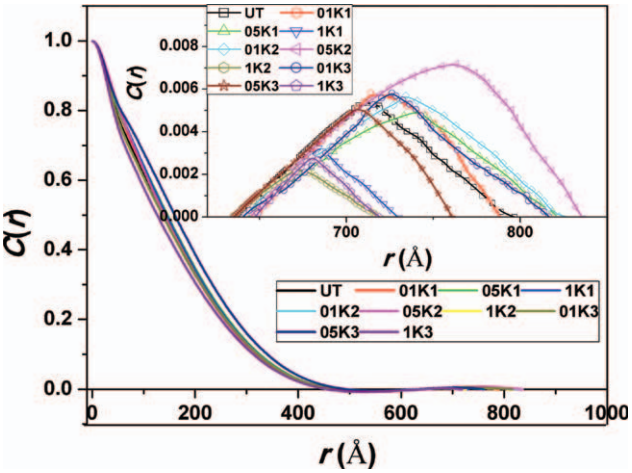

Figure 3. Variation of three dimensional correlation function $C(r)$ as a function of r for raw and $KMnO_4$-treated fibers. Inset: Magnified view of first subsidiary maximum of the three-dimensional correlation functions. [Color figure can be viewed in the online issue, which is available at wileyonlinelibrary.com.]

0.05% $KMnO_4$ acetone solution for 2 min (05K2) is found to have least void content and disorderness, i.e., "φ_2". However, the sample gets more disordered and void content starts to increase at higher concentrations and it becomes highest for 1K3. It may be due to the degradation of cellulosic material at higher concentrations with higher soaking periods because of the excessive oxidizing effect of $KMnO_4$ acetone solution.

The plots of $C(r)$ of all the investigated fibers are shown in Figure 3. The damping oscillatory behavior of the $C(r)$ for large values of r shows the nonideal two phase behavior of all the fiber samples. Another important parameter that is derived from the $C(r)$ is the length of coherence (l_c) (given in Table I) which gives the information about the distribution of electron across the boundary of the particle.

$$l_c = 2\int_0^\infty C(r)dr \tag{5}$$

According to Ruland[21] and Vonk[22] the information about the nonideal two phase system can be obtained from the parameter defined as "R" which was later modified by Mishra et al.[19] is as follows:

$$R = \frac{3}{2}\left(\frac{2\pi}{\lambda a}\right)^2 \frac{\int_0^\infty x^3\tilde{I}(x)dx}{\int_0^\infty x\tilde{I}(x)dx} \tag{6}$$

Where "R" is the corrugation at the phase boundary and "a" is the sample to detector distance.

If R goes to 8, the system is ideal but if it has some finite value the system becomes nonideal two phase. In this study, the values of R (shown in Table I) are found to be finite for all the investigated fibers which indicates that the electron density gradient is also finite for all the samples. Hence, all the fiber samples are nonideal two phase system.[22]

To find out the nature of the phase of the untreated and the treated fibers, logarithmic plots between the x and $\tilde{I}(x)$ values are drawn (Supporting Information Figure S1). The slopes of all the plots are found to be negative, which is ~ -3. This suggests that both the untreated and treated samples are nonideal, two phase system.[24]

In this study, the width of transition layers (E) is calculated by Ruland and Vonk method and is designated as E_r and E_v accordingly. The width of transition layer gives information about the corrugation at the phase boundary between the matter and void phase. Figure 4 displays the typical Ruland plots for all the investigated fibers, which is a graph of $\tilde{I}(x)\cdot x$ vs x^{-2}. The Ruland plots are obtained by taking 40 background corrected intensities. Linear fitting of each curves are carried out on 15 extreme points at the tail region of the corresponding curve. The functional relationship between $\tilde{I}(x)\cdot x$ and x^{-2} takes the form of

$$\tilde{I}(x)\cdot x = \frac{\pi C}{2\cdot(\lambda a)^3 - 2} - \frac{\pi^3 C}{3\cdot(\lambda a)\cdot E^2} \tag{8}$$

where C is the probability constant. The standard deviations (σ) of the intensities are well within the permissible range showing the accuracy of the data collection. The values of E_r obtained from Figure 4 are given in Table I.

The width of transition layer, E_v (Vonk method) is calculated by normalizing $C(r)$ to unity at the start of the real space. According to Vonk method,

$$\mathrm{E} = -\frac{4}{R}\left[\frac{dC(r)}{d(r)}\right]_r = E_y \tag{9}$$

The plot between $-\frac{4}{R}\left[\frac{dC(r)}{d(r)}\right]$ vs. r is shown in Figure 5. A straight line equidistance from both the axes has been drawn

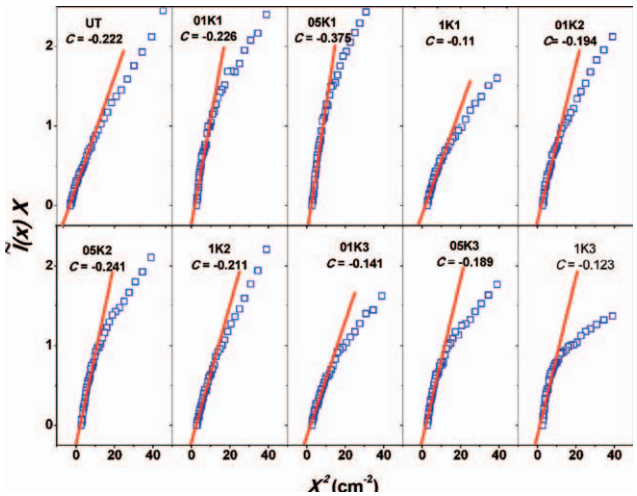

Figure 4. Ruland plots ($\tilde{I}(x)$ x vs. x^{-2}) of sisal fibers before and after $KMnO_4$ treatment to find out E_r of the respective fibers. [Color figure can be viewed in the online issue, which is available at wileyonlinelibrary.com.]

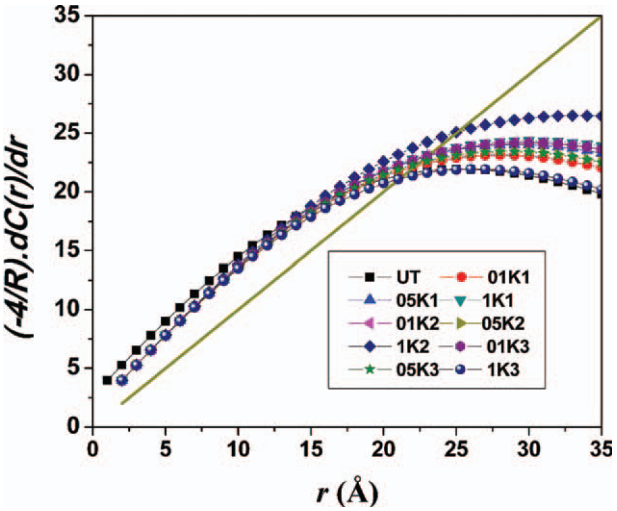

Figure 5. Variation of $\left(-\frac{4}{R}\right)\frac{dC(r)}{dr}$ against r for the raw and $KMnO_4$-treated sisal fibers to find out the E_v of the respective fibers. [Color figure can be viewed in the online issue, which is available at wileyonlinelibrary.com.]

and the point of intersection with the curve gives the values of E_v[22] for different fibers which are compiled in Table I. The values of E_r that are calculated from Figure 4 are in close agreement with the values of E_v evaluated from Figure 5. Hence, it justifies the accuracy of our analysis.

Finally the above SAXS computational analysis on all the sisal fibers confirms the fibers to be nonideal two phase system. Out of all the fibers, 05K2 fiber is found to have least void content and disorderness.

Figure 6 shows the XRD patterns of the untreated and $KMnO_4$-treated sisal fibers. The diffraction patterns are profile fitted by standard software. The crystallite sizes of the fibers were determined by modified Scherer's formula whereas the degrees of

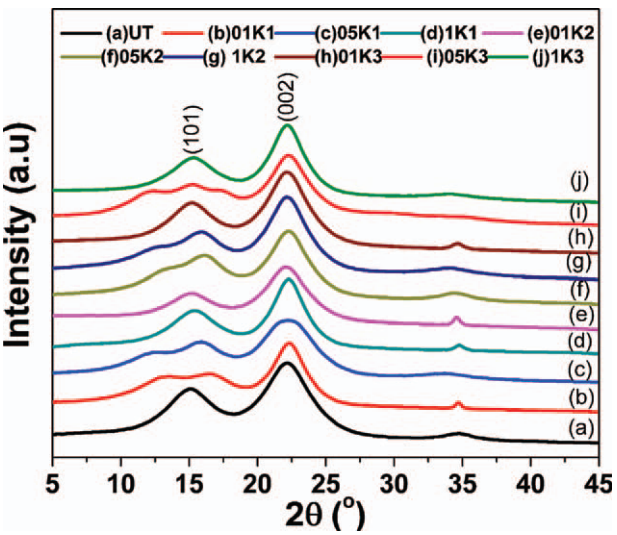

Figure 6. XRD patterns of sisal fibers before and after $KMnO_4$ treatment. [Color figure can be viewed in the online issue, which is available at wileyonlinelibrary.com.]

Table II. Various Crystallographic and Physical Parameters of the Investigated Raw and $KMnO_4$-Treated Sisal Fibers

Fiber	Degree of crystallinity (%)	Crystallite size (A^O)	Density (g/cc)
UT	52.11	29.19	1.32
01K1	53.01	31.42	1.39
05K1	58.22	33.18	1.50
1K1	50.01	26.85	1.29
01K2	56.09	32.18	1.43
05K2	59. 93	33.93	1.61
1K2	49.29	25.77	1.25
01K3	52.16	30.47	1.34
05K3	51.22	27.93	1.30
1K3	45.91	22.09	1.20

crystalinity were calculated by Segal's empirical method.[20] All these crystallographic structural parameters are shown in Table II. The highest degree of crystalinty for the 05K2 is shown by maximum increase in the intensity of the crystalline peak at 22.5° followed by 05K1 and is least for 1K3. The particular concentration of $KMnO_4$ at 05K1 and 05K2 may have able to effectively oxidize the sisal fiber surface and etch out lignin binding thousands of micro-fibrils together inside the fiber.[25] It helps in removing the noncrystalline material from the fiber and making the interfibrilar region less dense and less rigid there by allowing cellulose microfbiril to rearrange in a more compact manner. This may have lead to the increment in the degree of crystalinty. Whereas at a higher soaking period and higher concentration of $KMnO_4$ acetone solution, the removal of cellulosic material along with the lignin takes place resulting in decrease of degree of crystalinity. The increase in the dimension and size of the crystallites of 05K2, 05K1 as shown in Table II may be due to the decrease in crystal distortion and defects.[26] It also leads to increase in bulk fiber density.

Figure 7 exhibits the FTIR Spectra of the untreated and $KMnO_4$-treated sisal fibers. The broad absorbance peak at 3200–3400 cm^{-1} range corresponds to the O—H stretching of hydrogen bond network. This peak tends to decrease with the increment in the soaking period of the fiber in $KMnO_4$-acetone solution from 1 to 2 min. It suggests that the hydroxyl stretching vibration decreases due to longer period of treatment. The decrement in intensities becomes prominent in case of 05K2 followed by 05K1. It suggests that at this particular concentration and time the $KMnO_4$ effectively oxidizes the sisal fiber and breaks the hydrogen bond between the O—H groups of cellulose and hemicelluloses. But at higher concentration, i.e., at 0.1% the intensities of O—H group tends to increase because of the degradation of cellulose and incorporation of more polar groups.[13] Hence at 1K3 the O—H group is highest. The peaks at 2900 and 2850 cm^{-1} are also seem to be affected by $KMnO_4$ treatment which are the characteristic peak of C—H stretching vibration of methyl group of methylene and wax, respectively. The intensities at these two peaks are found to be least for 05K2 which confirms the substantial removal of wax from the

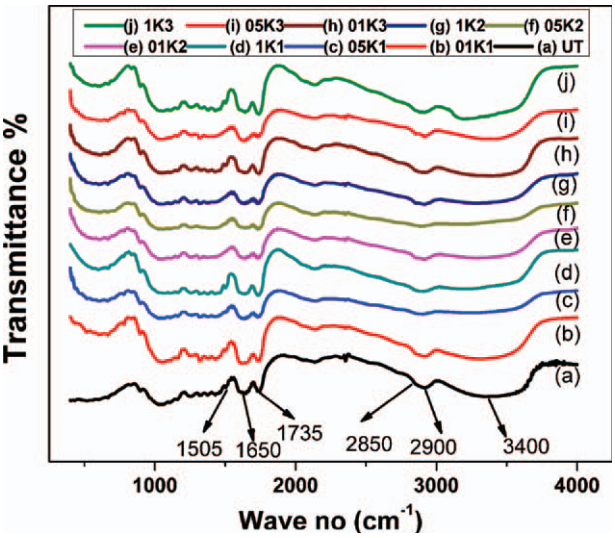

Figure 7. IR spectra of raw and $KMnO_4$-treated sisal fibers. [Color figure can be viewed in the online issue, which is available at wileyonlinelibrary.com.]

fiber due to the treatment. The peaks at 1735 and 1650 cm^{-1} which correspond to C=O stretching in carbonyl, unsaturated β-keton and absorbed water are found to be decreased remarkably at 05K2. The lignin peak at 1505 cm^{-1} is also decreased showing that $KMnO_4$ has effectively etched out lignin from the fiber surface at this particular concentration and soaking period. But at the higher treating period like 3 min for the same concentration, the degradation of the fiber starts which is due to the excessive oxidation. This may be due to the degradation of cellulose inside the fiber and sedimentation of wax on the fiber by the subsequent reaction for which the peak at 2900 cm^{-1} and 2850 cm^{-1} were appeared again.

The longitudinal surface morphologies of UT, 05K2, and 1K3 sisal fibers are shown in the Figure 8(a–c), respectively. It is observed that the surface roughness of the 05K2 fiber has been increased significantly after the $KMnO_4$ treatment which may be due to fibrillation of the fiber due to the removal of lignin along with the impurities from the fiber.[25] Figure 8(d–f) show the fractured surfaces of the UTC and 05KC2 and 1K3, respectively. Because of the increased surface area and roughness of the fiber after $KMnO_4$ treatment the adhesion between fiber and the matrix has increased which is very much clear from the SEM micrographs. The adhesion is so strong that it is marked by traces of matrix on the surface of the fiber in the fractured region. This may be due to the initiation of graft co-polymerization by highly reactive MnO_3^- ion as explained below.[27] Here the OH groups inside the fiber get oxidized.

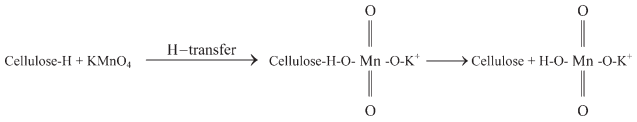

However the gap around the fiber at the interface in the UTC shows the poor adhesion between untreated sisal fiber and the matrix. The excessive oxidation of the fiber at higher concentration and longer period of treatment also leads to the composites with weak interface which is shown in Figure 8(f).

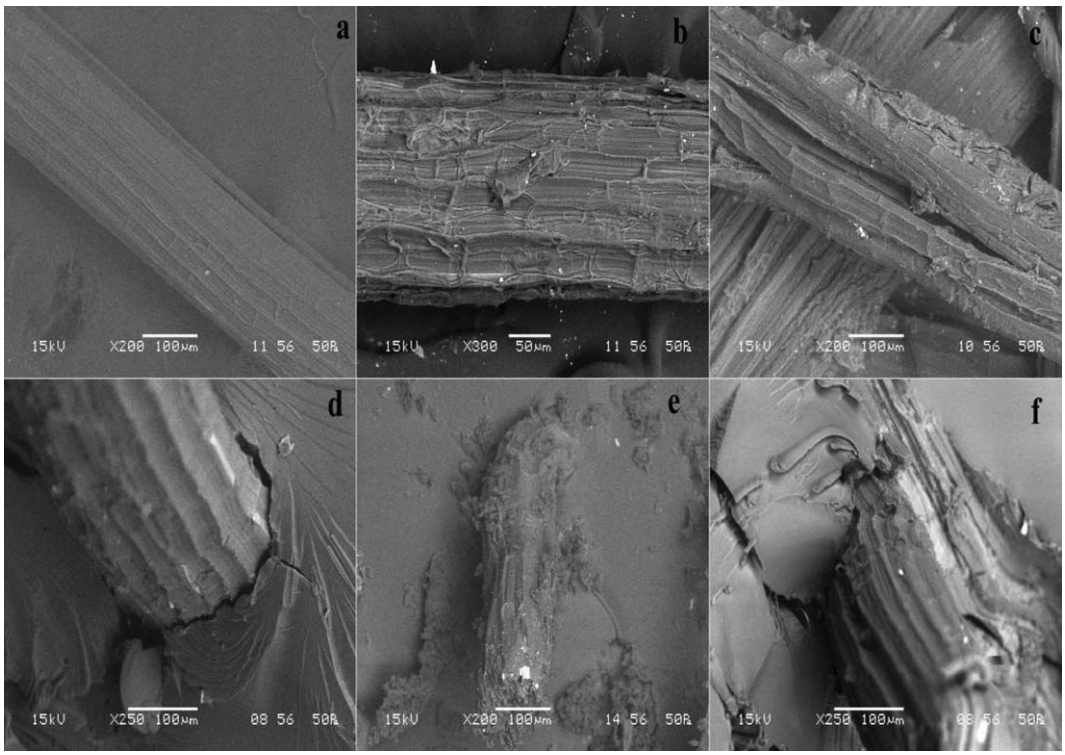

Figure 8. (a–c) Longitudinal morphology of raw and 05K2 and1K3 fibers. (d–e) Fractured surface of UTC and 05KC2 and1KC3 composites, respectively.

Applied Polymer SCIENCE

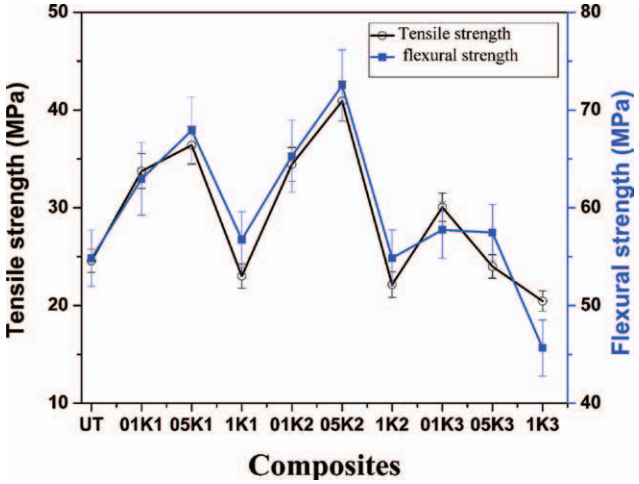

Figure 9. Flexural and tensile strengths of UTC and KSFREC. [Color figure can be viewed in the online issue, which is available at wileyonlinelibrary.com.]

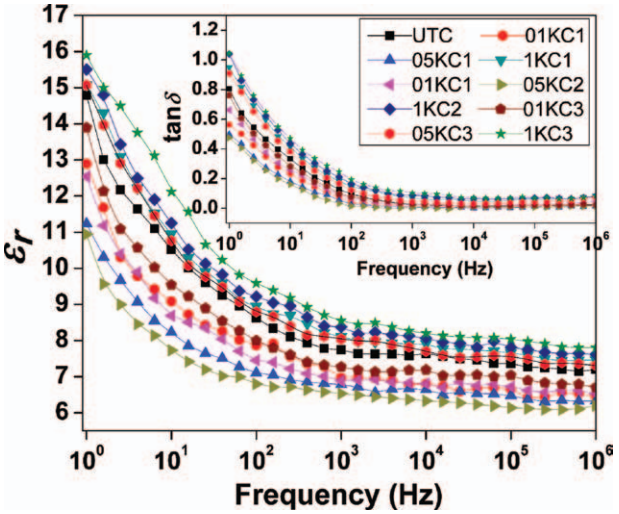

Figure 10. Variation of ε_r with frequency for UTC and KSFREC. Inset: Variation of tanδ with frequency for UTC and KSFREC. [Color figure can be viewed in the online issue, which is available at wileyonlinelibrary.com.]

The flexural strength and tensile strength of UTC and KSFREC are shown in Figure 9. It is established that the interfacial zone plays a leading role in transferring the load between fiber and matrix in fiber-reinforced composite system, which consequently affects the mechanical properties such as strength.[28] The flexural failure depends mainly on the fiber-matrix adhesion. The flexural strength and the tensile strength of the 05KC2 are found to be the highest and are followed by 05KC1. The increased surface area and roughness due to the removal of impurities and waxy layer in these samples facilitates the mechanical interlocking between fiber and the resin.[29] This is further confirmed from the SEM micrograph as shown in Figure 8. But at a higher concentration, because of the excessive oxidation of the fiber surface by $KMnO_4$ the strength providing cellulosic gets degraded along with the lignin and waxy material present in fiber. This may have lead to the poor mechanical strength of the composite. It justifies the previous finding that the concentration of $KMnO_4$ has significant effect on the fiber and hence on the fiber reinforced composite.[30] The degradation of the mechanical strength becomes more intense with increase in soaking period at higher concentration which is clear from the Figure 9.

Figure 10 displays the frequency dependence of dielectric constant (ε_r) of both UTC and KSFREC. Inset of the above figure shows the frequency dependence of dielectric loss (tan δ). It is found that with the increase in frequency the value of ε_r as well as tan δ decreases. The change of ε_r and tan δ at lower frequency region is higher than that at very high frequency. Generally, ε_r of a polymeric material depends mainly on interfacial and dipole polarization. The interfacial polarization is prominent in heterogeneous material and is highest at lower frequency. Hence, the higher values of ε_r and tan δ at lower frequency can be explained in terms of interfacial polarization and the free motion of dipoles within the material which is connected to ac conductivity relaxation. It is found that the values of ε_r of the investigated composites follows the trend of 05KC2<05KC1<01KC2<01KC1<01KC3<UTC<05KC3<1KC1 <1KC2<1KC3. It may be due to the increase in the degree of crystalinity because of the removal of noncrystalline part of the fiber. The overall dielectric properties in a polymeric composite are the contribution of both the crystalline and amorphous content of the composite. Amorphous content makes the major contribution to both ε_r and tan δ. As a result, ε_r and tan δ decreases with an increasing degree of crystallinity.[31] Therefore 05KC2 has the least values of ε_r and tan δ. However at higher concentration the value ε_r tends to increase even above the value of ε_r of UTC. It becomes highest for the maximum soaking time at this concentration, i.e., at 1KC3. The higher concentration of the $KMnO_4$-acetone solution tries to degrade the strength providing cellulose part in the fiber and hence creating more polar group resulting in higher values ε_r and tan δ.

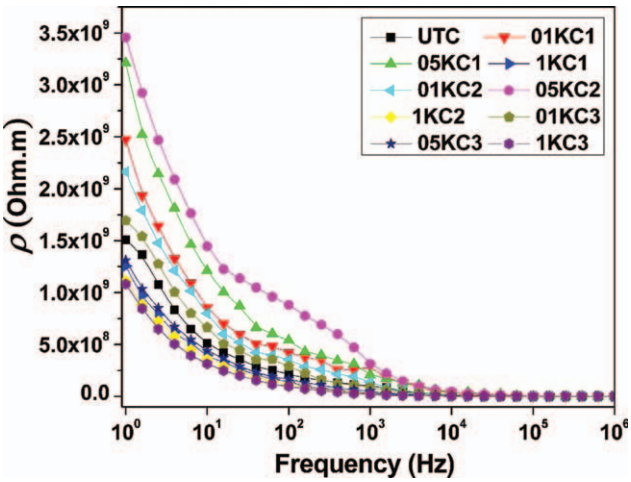

Figure 11. Variation of ρ with frequency for UTC and KSFREC. [Color figure can be viewed in the online issue, which is available at wileyonlinelibrary.com.]

The removal of lignin, hemicelluloses and impurities lead to the improvement in the surface area of the reinforcing fiber which leads to the better contact of the fiber with the matrix. The better interlocking between the fibers and matrix might have hindered the free molecular motion of the molecular chain in the composite interface leading to the increase in the volume resistivity of 05KC2 composite as shown in Figure 11.

CONCLUSIONS

The macromolecular study on the raw and $KMnO_4$-treated sisal fibers by SAXS analysis suggests that 05K2 fiber has less void content showing the least disorderness among all the investigated fibers. The degree of crystalinity, crystallite size, and bulk density are found to be highest for the above mentioned fiber. Maximum reduction of OH group and lignin content are observed for the 05K2 sample followed by 05K1. Enhancement of the surface roughness and better wetting of 05K2 fibers in the epoxy has been confirmed from the SEM micrograph. The highest mechanical strength, i.e., flexural and tensile strength for 05KC2 are due to the better mechanical interlocking of the fiber with the matrix. The lowest value of ε_r and tan δ for the above mentioned composite may be due to the reduction of OH group and rigid interface between the fiber and matrix. The highest value of ε_r in case of 1KC3 may be due to the increase in the polar group due to the degradation of the cellulose because of the excessive oxidizing effect of $KMnO_4$ at a higher concentration with higher soaking time. This study optimizes the modification process of the fiber by $KMnO_4$. Finally it is concluded that the 0.05% of $KMnO_4$-acteone solution is the best to modify the sisal fiber surface if it is immersed in the solution for 2 min to have a better tensile and flexural strength with low loss, least ε_r and higher volume resistivity.

This work was partly supported by CSIR, sanction.no.09/983(0006)/2010-EMR-I, India. The authors wish to acknowledge the Director, Defence Metallurgical Research laboratory, India for the provision of small angle X-ray scattering. They are also thankful to Prof. Pawan kumar, Department of Physics, NIT Rourkela, India for rendering the LCR meter facility for electrical characterization. The authors want to express their gratitude to Dr. Md. N. Khan, IGIT, Sarang, India, for his support during the analysis of SAXS data.

REFERENCES

1. Spinace, M. A. S.; Lambert, C. S.; Fermoselli, K. K. G.; De Paoli, M. A. *Carbohydr. Polym.* **2009,** *77*, 47.
2. Patra, A.; Bisoyi, D. K. *J. Mater. Sci.* **2010,** *42*, 5742.
3. Mylsamy, K.; Rajendran, I. *Mater. Des.* **2011,** *32*, 4629.
4. Corrales, F.; Vilaseca, F.; Llop, M.; Girones, J.; Mendez, J. A.; Mutje, P. *J. Hazard. Mater.* **2007,** *144*, 730.
5. Mominul, H. M.; Hasan, M.; Saiful Islam, M.; Ershad, A. M. *Bioresour. Technol.* **2009,** *100*, 4903.
6. Toki, S.; Sics, I.; Ran, S.; Liu, L.; Hsiao, B. S. *Polymer* **2003,** *44*, 6003.
7. Kelarakis, A.; Yoon, K.; Sics, I.; Somani, R. H.; Hsiao, B. S.; Chu, B. *Polymer* **2005,** *46*, 5103.
8. Bal, S.; Behera, R. C. *IJEMS* **2007,** *14*, 240.
9. Kalia, S.; Kaith, B. S.; Kaur, I. *Polym. Eng. Sci.* **2009,** *49*, 1253.
10. George, J.; Bhagawan, S. *Compos. Interf.* **1998,** *5*, 201.
11. Paul, P. A.; Oommen, C.; Joseph, K.; Mathew, G.; Thomas, S. *Polym. Compos.* **2010,** *31*, 113.
12. Khan, M. A.; Hassan, M.; Taslima, R.; Mustafa, A. I. *J. Appl. Polym. Sci.* **2006,** *100*, 4361.
13. Paul, A.; Joseph, K.; Thomas, S. *Compos. Sci. Technol.* **1997,** *51*, 67.
14. Wolfgang, G.; Martinschitz, K. J.; Boesecke, P.; Keckes, J. *Compos. Sci. Technol.* **2006,** *66*, 2639.
15. Patra, A.; Bisoyi, D. K. *J. Mater. Sci.* **2011,** *46*, 7206.
16. Roy, S. C. *Text Res. J.* **1960,** *30*, 451.
17. Ratho, T.; Torasia, S.; Mohanty, J. C. *Ind. J. Phys.* **1964,** *38*, 28.
18. Khan, MD.N. Ph.D. thesis, **1991**, NIT Rourkela, India.
19. Mishra, T.; Bisoyi, D. K.; Patel, T.; Patra, K. C.; Patel, A. *Polym. J.* **1988,** *20*, 739.
20. Segal, L.; Creely, J.; Martin, J. A. E.; Conrad, C. M. *Text. Res. J.* **1959,** *29*, 786.
21. Ruland, W. *J. Appl. Cryst.* **1971,** *4*, 70.
22. Vonk, C. G. *J. Appl. Cryst.* **1975,** *8*, 340.
23. Vilay, V.; Mariatti, M.; Mat Taib, R.; Todo, M. *Compos. Sci. Technol.* **2008,** *68*, 631.
24. Prasad, N.; Patnaik, J.; Bohidar, N.; Mishra, T. *J. Appl. Poly. Sci.* **1998,** *67*, 1753.
25. Yan, L.; Chunjing, H.; Yehong, Y. *Compos. Part A* **2008,** *39*, 570.
26. Liansong, W.; Dongling, H.; Tianyao, Z.; Lifang, Z.; Chengdong, X. *Cryst. Res. Technol.* **2010,** *45*, 275.
27. Moharana, S.; Mishra, S. B.; Tripathy, S. S. *J. Appl. Polym. Sci.* **1990,** *40*, 354.
28. Georgopoulos, S. T.; Tarantili, P. A.; Avgerinos, E.; Andreopoulos, A. G.; Koukios, E. G. *Polym. Degrad. Stabil.* **2005,** *90*, 303.
29. Franco, P. J.; Valadez-Gonzalez, A. *Compos. Part B* **2005,** *36*, 597.
30. Joseph, K.; Thomas, S.; Pavithran, C. *Polymer* **1996,** *37*, 5139.
31. Hanna, A. A.; Atef, A. I.; Salwa, O.; Heikal, S. O. *J. Polym. Sci. Polym. Chem. Ed.* **1980,** *18*, 1425.